Volume 14
Number 8
21 April 2024
Pages 2015–2308

Catalysis Science & Technology

rsc.li/catalysis

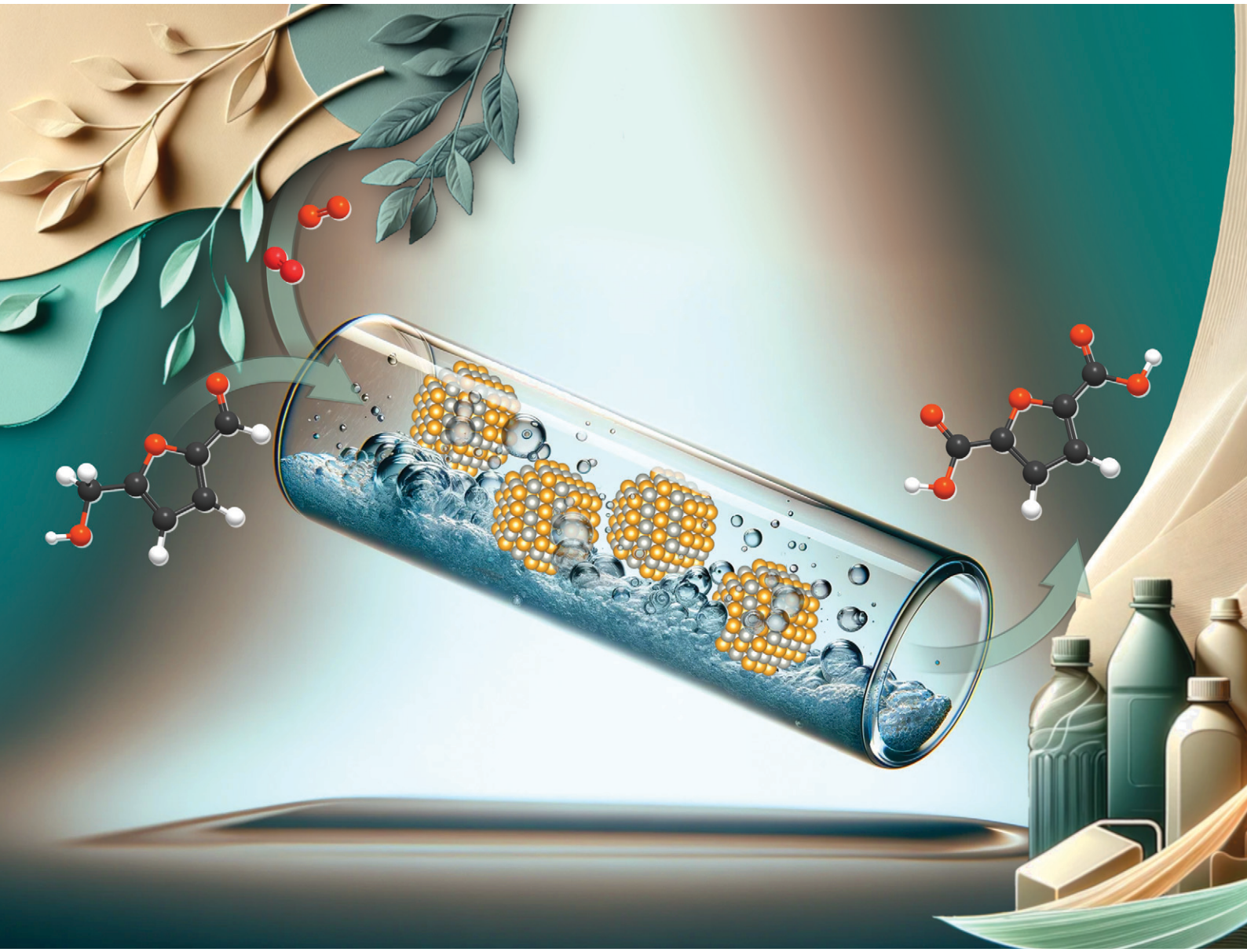

ISSN 2044-4761

ROYAL SOCIETY OF CHEMISTRY

PAPER
Erisa Saraçi *et al.*
Continuous flow oxidation of HMF using a supported AuPd-alloy

Catalysis Science & Technology

ROYAL SOCIETY OF CHEMISTRY

PAPER

View Article Online
View Journal | View Issue

Cite this: *Catal. Sci. Technol.*, 2024, **14**, 2130

Continuous flow oxidation of HMF using a supported AuPd-alloy†

Dominik Neukum, [a] Ajai R. Lakshmi Nilayam,[cd] Maya E. Ludwig,[a] Athanasios A. Vadarlis,[a] Jan-Dierk Grunwaldt [ab] and Erisa Saraçi *[ab]

Received 13th December 2023,
Accepted 24th February 2024

DOI: 10.1039/d3cy01722b

rsc.li/catalysis

The oxidation of 5-(hydroxymethyl)furfural (HMF) to 2,5-furandicarboxylic acid (FDCA) holds significant promise for replacing fossil-based monomers. Continuous flow operation enhances the process in terms of green chemistry by improving heat and mass transfer, enabling easier scalability of the reaction and ensuring higher safety with a smaller reactor volume. In this study, we investigated the use of heterogeneous catalysts in a fixed-bed reactor for the continuous oxidation of HMF. Air served as a green oxidant, water as a non-toxic solvent, and Na_2CO_3 as a mild base. An AuPd-alloy-based catalyst supported on activated carbon demonstrated remarkable performance, yielding 81% FDCA at a liquid hourly space velocity of 31.4 h^{-1}. This corresponds to a productivity of 68 mol_{FDCA} mol_{AuPd}^{-1} h^{-1}, which is, to our knowledge, one order of magnitude higher than typically reported for the heterogeneously catalyzed continuous oxidation of HMF. In addition, the catalyst showed a good stability over 90 h time on stream without any detectable deactivation. The formation of humins led to a progressive catalyst deactivation. The developed catalytic system and continuous process offer a more sustainable and efficient approach to future production of the renewable monomer FDCA.

Introduction

The production of renewable monomers, which are key products in the chemical industry, is of great interest to transition towards a bio-based chemical industry.[1–3] The use of biomass brings a substantial opportunity, leveraging inherent functional groups that only necessitate simple transformation, instead of introducing such groups *via* oxidation of fossil-based hydrocarbons.[3,4] The effective H/C-ratio of bio-derived base chemicals is closer to that of the desired monomer products, in comparison to their fossil-derived counterparts, reducing the amount of transformation steps and fostering more sustainable processes.[3,5] The oxidation of 5-(hydroxymethyl)furfural (HMF), ideally sourced from lignocellulose or other biomass sources, to yield 2,5-furandicarboxylic acid (FDCA) emerges as a promising avenue for the production of renewable monomers.[6–10] FDCA can be used to produce various polyesters, particularly as a substitute for fossil-derived terephthalic acid.[11,12] The oxidation of HMF has been explored through various approaches, encompassing stoichiometric reagents, homogeneous catalysts, heterogeneous catalysts, and bio-catalysts.[1,13–15] In the context of sustainability, heterogeneous catalysts emerge as the preferred choice due to their facile separation from the reaction medium, effective reusability, and high stability.[16] Extensive investigations employing both non-noble and noble metal-based catalysts have been reported.[1,13,17,18] Despite the higher cost associated with noble metal-based catalysts, their superior activity and stability, coupled with the utilization of air as a green and safe oxidant make them compelling candidates.[6,19–21] A list of noble metals, including Au,[6,7,19,22,23] Pt,[20,24–26] Pd,[27,28] Ru,[29–31] and Ag,[32,33] and various bimetallic combinations[8,21,34–38] have been reported for the oxidation of

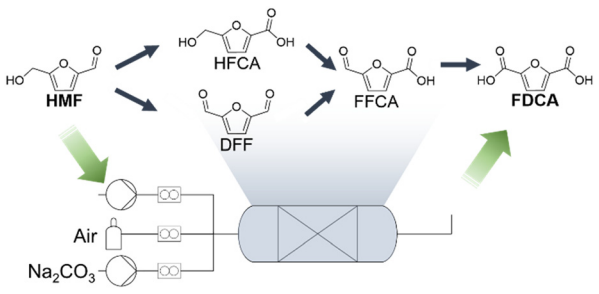

Scheme 1 Simplified reaction mechanism and reactor scheme for HMF oxidation.[1]

[a] *Institute of Catalysis Research and Technology, Karlsruhe Institute of Technology, Hermann-von-Helmholtz-Platz 1, 76344 Eggenstein-Leopoldshafen, Germany. E-mail: erisa.saraci@kit.edu*
[b] *Institute for Chemical Technology and Polymer Chemistry, Karlsruhe Institute of Technology, Engesserstraße 20, 76131 Karlsruhe, Germany*
[c] *Institute of Nanotechnology, Karlsruhe Institute of Technology, Hermann-von-Helmholtz-Platz 1, 76344 Eggenstein-Leopoldshafen, Germany*
[d] *Karlsruhe Nano Micro Facility (KNMFi), Karlsruhe Institute of Technology, Hermann-von-Helmholtz-Platz 1, 76344 Eggenstein-Leopoldshafen, Germany*

† Electronic supplementary information (ESI) available: Additional experimental information, characterization and catalytic testing. See DOI: https://doi.org/10.1039/d3cy01722b

HMF. Their successful deployment not only attests to their catalytic efficiency but also aligns with a closed-cycle approach, wherein the catalysts exhibit reusability and end-of-life noble metals can be recycled for subsequent catalyst preparation.[39]

The oxidation of HMF can proceed *via* two different reaction routes depending on the alkalinity of the reaction medium and the active metal species involved.[6,37,40,41] The initial oxidation step targets either the alcohol or the aldehyde functional group (Scheme 1), resulting in the formation of 5-(hydroxymethyl)furan-2-carboxylic acid (HFCA) or 2,5-diformylfuran (DFF). Subsequent oxidation leads to 5-formyl-2-furancarboxylic acid (FFCA) and finally FDCA.

Despite the vast knowledge on HMF oxidation with heterogeneous catalysts, most studies have been confined to batch processes, although continuous processes offer various advantages, especially in the context of green chemistry. The adoption of continuous flow synthesis presents several advantages, including easier scalability, improved heat and mass transfer favouring energy efficiency, and a safety enhancement due to reduced reactor volume, mitigating the risk of runaway reactions.[42–44] Recognizing these merits, continuous flow synthesis has been acknowledged by the International Union of Pure and Applied Chemistry (IUPAC) as one of ten chemical innovations contributing to a sustainable future.[45,46] Despite the obvious advantages, reports on the continuous flow oxidation of HMF utilizing heterogeneous catalysts are very scarce. Lilga *et al.* studied the continuous oxidation of HMF with Pt-based catalysts in a tubular reactor, noting the highest reaction rates for the formation of FDCA with an alkaline feed compared to neutral and acidic solutions.[47] They observed a high initial selectivity to FDCA, which decreased slightly over the following hours of time on stream (ToS). The FDCA yield increased with an increase of pressure or gas hourly space velocity (GHSV), or a decrease of the liquid hourly space velocity (LHSV). Similar observations were made for the continuous oxidation of HMF with a Ru/Al_2O_3 catalyst, however, only a moderate FDCA yield of 63 ± 2% was obtained.[48] An enhancement of the FDCA yield with higher reaction temperature up to 140 °C was found. Motagamwala *et al.* used a 1 : 1 mixture of H_2O and γ-valerolactone as solvent for the continuous oxidation, resulting in an improved solubility of FDCA, which reduces the risk of blocking active sites.[26] A good stability of the Pt/C catalyst with an average FDCA yield of about 94% over 60 h ToS was achieved. Finally, base-free conditions with Pt supported on a resin were explored, yielding 99% FDCA over 44 h ToS.[49] However, limited HMF-concentration (0.025 M) was used to avoid precipitation of FDCA, lowering the FDCA productivity considerably.

In our study, we systematically explore the oxidation of HMF in a continuous flow reactor utilizing AuPd-based catalysts renowned for their efficacy in achieving high FDCA yields in batch reactors.[21,34,37,38,50] We implemented air as a sustainable and economical oxidant, water as a safe and green solvent, Na_2CO_3 as a mild and non-toxic base, and heterogeneous catalysts in a fixed-bed reactor to avoid separation of the catalytic system from the reaction mixture. These measures collectively enable a more sustainable approach to the production of the important renewable monomer FDCA. Our investigation delves into the influence of support materials, reaction temperature, pressure, and base-equivalents on the oxidation process, providing comprehensive insights into the key factors that influence the efficiency of the oxidation reaction, thereby informing strategies for optimizing FDCA production. A critical facet of our study involves the assessment of the long-term stability of the catalytic system, which is of utmost importance for ensuring the sustainability of the entire process.

Experimental

Catalyst synthesis

AuPd-alloyed particles with a targeted ratio of 52 : 48 (Au : Pd) were prepared according to a method previously published by our group.[21] In brief, $PdCl_2$ (m = 0.0222 g) and $HAuCl_4{\cdot}3H_2O$ (m = 0.0533 mg) were dissolved in diluted HCl (3 mL conc. HCl in 77 mL H_2O) for about 3 h. Subsequently, 620 mL H_2O and poly(vinylalcohol) (PVA; m = 37.8 mg) were added. The solution was stirred for 10 min and then a diluted $NaBH_4$ (m = 39.4 mg) solution was added. After an additional 30 min of stirring, the pH of the solution was adjusted by addition of either 50 vol% H_2SO_4 or KOH (activated carbon (AC-ROX): pH = 13, ZrO_2: pH = 1, TiO_2: pH = 1). Following this, the support material (m = 1.96 g) was added to the suspension corresponding to a AuPd-loading of 2 wt%. The catalyst was subjected to overnight stirring before being separated from the solution *via* filtration. The catalyst was thoroughly washed and dried overnight.

Characterization methods

X-ray diffraction (XRD). XRD of the catalysts was performed on a PANalytical X'Pert Pro diffractometer with Cu-K_α radiation and a Ni-filter. The data was recorded in a 2θ range of 5–120° ($AuPd/ZrO_2$, $AuPd/TiO_2$) and 20–80° (AuPd/AC-ROX) with a step size of 0.017°. The final diffractograms were obtained by summing up 2 scans (AuPd/AC-ROX) and 8 scans ($AuPd/ZrO_2$, $AuPd/TiO_2$).

Inductively coupled plasma-optical emission spectrometry (ICP-OES). Digestion of the catalysts for ICP-OES was carried out in a mixture of 6 mL conc. H_2O_2, 2 mL conc. HNO_3 and 4 mL conc. HCl. Microwave irradiation of 600 W was applied for 90 min. The solution was diluted to a volume of 25 mL before being measured in an Agilent 725 spectrometer with a plasma excitation of 49 MHz and 2 kW.

Scanning transmission electron microscopy (STEM). STEM images and selected area electron diffraction (SAED) of the supported catalysts were taken with a ThermoFisher Themis 300 (S)TEM equipped with a high-angle annular dark-field (HAADF) detector (convergence angle: 8.6 mrad, 30 mrad; collection angle: 77–200 mrad). A standard lacey carbon grid with Cu mesh was used for preparation of the catalyst samples. We did not consider agglomerated particles for the particle size

distribution. The particle size was evaluated with ImageJ. Energy dispersive X-ray (EDX) images were recorded with a ThermoFisher Scientific Super-X EDX detector (convergence angle: 30 mrad, collection angle range: 62–200 mrad). STEM raw data can be found at **https://doi.org/10.35097/1938**.

Continuous flow oxidation of HMF

The catalyst was loaded into a tubular reactor with a 3/8-inch diameter, preheated to the specified reaction temperature before introducing the reactant solution. The aqueous HMF-solution with a concentration of 0.2 M and the aqueous Na_2CO_3-solution were pumped separately into the reactor at identical flow rates, resulting in a final HMF concentration of 0.1 M within the reactor. Upon mixing of the two aqueous streams, air was introduced at the given flow rate and reaction pressure. The product solution was collected after the backpressure regulator, and samples for HPLC analysis were collected. In certain instances, solid impurities in the HMF-solution caused fluctuations in the flow rate inducing variations in observed product yields. Hence, averaged product yields and productivities after reaching a steady state were compared to account for fluctuations in the HMF-concentration in the feedstock. The measurement of the ToS started when the reactants reached the reactor. Additional information on the experimental setup can be found in the ESI.†

Results and discussion

Characterization

The metal loading for each of the tested catalysts was determined by ICP-OES (Table 1). The total metal loading varied between 1.4 wt% ($AuPd/ZrO_2$ and AuPd/AC-ROX) and 1.7 wt% ($AuPd/TiO_2$). The deviation from the targeted loading of 2 wt% might be attributed to the supporting process of the particles. Apart from $AuPd/ZrO_2$, which had a Au : Pd ratio of 49 : 51, the nanoparticles generally displayed a slightly higher Au content compared to the intended ratio of 52 : 48. Nevertheless, the discrepancy was marginal for all the catalysts, and no significant differences in catalytic activity were anticipated due to these variations.[21]

All the catalysts showed comparable and narrow particle size distributions (Fig. 1) with mean particle diameters ranging from 3.3 nm to 4.2 nm (Table 1). Particle agglomeration was observed on the activated carbon support (AC-ROX). In the case of TiO_2 and ZrO_2, predominantly isolated particles were found in the STEM images. The particles showed a homogeneous distribution of Au and Pd in the EDX-mapping (Fig. S3†).

X-ray diffraction analysis was employed to identify reflections indicative of metallic AuPd-alloys, confirming the successful alloy formation (Fig. S4†). For AuPd/AC-ROX, the presence of alloyed AuPd-particles with a broad reflection at 39.04° was found, aligning with the intended 1 : 1 ratio in the AuPd-alloys. In the case of $AuPd/ZrO_2$ and $AuPd/TiO_2$, the alloy reflections were overlaid by the reflections from the respective support materials. Specifically, the TiO_2-based catalyst showed a combination of anatase and rutile phases, while the reflections of Au/ZrO_2 were assigned to a monoclinic ZrO_2-phase.

To further confirm the alloy formation at the level of an individual nanoparticle, a SAED pattern of a single AuPd nanoparticle on AuPd/AC-ROX was recorded (Fig. 2). The diffraction pattern of the particle could be assigned to the crystal planes in the fcc-structure of a AuPd (1 : 1) reference (ICSD collection code 58571). The determined lattice constant of 0.396 nm closely approximated the reference data with 0.398 nm (ICSD collection code 58571). The detailed analysis was only feasible for AuPd/AC-ROX, as the other two catalysts predominantly showed reflections of the metal oxide supports.

Table 1 Metal loading, metal ratio and mean particle diameter of $AuPd/ZrO_2$, $AuPd/TiO_2$, and AuPd/AC-ROX as determined by ICP-OES and STEM

Catalyst	Au-loading/wt%	Pd-loading/wt%	$n_{Au} : n_{Pd}$	$\bar{d}_{particle}$/nm
$AuPd/ZrO_2$	0.9 ± 0.1	0.5 ± 0.1	49 : 51	3.3 ± 1
$AuPd/TiO_2$	1.2 ± 0.1	0.5 ± 0.1	56 : 44	4.2 ± 0.9
AuPd/AC-ROX	1.0 ± 0.1	0.4 ± 0.1	57 : 43	3.5 ± 0.9

Catalytic testing in batch mode

Before subjecting the catalysts to continuous flow testing, a comprehensive investigation of all the catalysts was conducted in the batch oxidation of HMF (0.1 M HMF, 100 °C, 15 bar air, 2 eq. Na_2CO_3, 5 h, M : HMF 1 : 92). All the catalysts were used in powder form in these preliminary assessments (Table 2). Each catalyst demonstrated a quantitative conversion of HMF under the tested reaction conditions. AuPd/AC-ROX showed the highest FDCA yield, achieving a quantitative conversion of HMF to FDCA, thus representing the most proficient catalyst in these batch tests. $AuPd/TiO_2$ and $AuPd/ZrO_2$ followed with FDCA yields of 97% and 94%, respectively. In their powder form, all three catalysts delivered high yields of FDCA in the batch process. However, the catalytic activity exhibited variations in continuous flow testing, highlighting the importance of understanding how these catalysts function under dynamic, continuous conditions.

Comparison of catalysts in continuous flow

In the assessment of catalysts for continuous flow oxidation of HMF, TiO_2, ZrO_2, and AC-ROX were employed as support materials to identify the most suitable catalyst. Fig. 3 displays the FDCA yield as a function of ToS for the three catalysts, revealing a striking distinction with AuPd/AC-ROX achieving the highest FDCA yield with a maximum over 90%. The other two catalysts followed in the order of $AuPd/TiO_2$ and $AuPd/ZrO_2$, presenting similar FDCA yields.

Previous work by Lilga *et al.*[47] observed the highest FDCA-productivity for inorganic metal oxides with a low surface area. The use of carbon-based supports led to product inhibition due to the strong adsorption of HMF and the

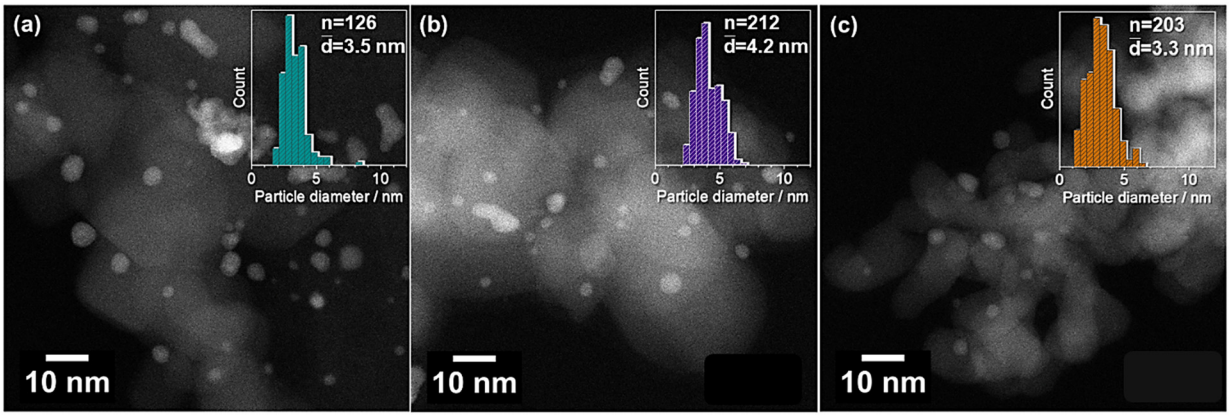

Fig. 1 STEM images and particle size distributions (inset: particle size distribution, *n*: particle count, *d*: average particle diameter) of (a) AuPd/AC-ROX (n = 126), (b) AuPd/TiO_2 (n = 212), and (c) AuPd/ZrO_2 (n = 203).

oxidized products. Nevertheless, AC-ROX was shown in the literature to play an active role in the base-free HMF-oxidation, possessing good adsorption properties for HMF, which potentially increases the catalytic activity in continuous flow oxidation under alkaline conditions.[51]

AuPd/AC-ROX emerged as the superior catalyst, giving the highest average FDCA yield at 87%, in contrast to 74% for AuPd/TiO_2 and 61% for AuPd/ZrO_2 (Fig. 3). Furthermore, AuPd/TiO_2 and AuPd/ZrO_2 demonstrated the tendency to form humins at higher flow rates, resulting in lower FDCA yields, rendering them less suitable for increasing the overall productivity. The different density of the support materials resulted in a variation of the LHSV for all tested catalysts. AuPd/AC-ROX achieved higher FDCA yields even at higher LHSV compared to the other two catalysts. Over a range of 5.3 h^{-1}, which is close to the LHSV of AuPd/TiO_2, up to 16.3 h^{-1} an average FDCA yield >89% was achieved (Fig. S5†). Only for the highest tested LHSV of 31.4 h^{-1} a drop in the average FDCA yield to 63.2% was visible. This proves the superior intrinsic catalytic activity of AuPd/AC-ROX over a broad LHSV range. The higher catalytic activity might originate from the superior adsorption properties of AC-ROX,[51] particularly for HMF, which was not adsorbed on the surfaces of TiO_2 and ZrO_2 (Table S2†). AC-ROX thus proved to be the most suitable support material for further testing, offering the potential to enhance the productivity of FDCA further.

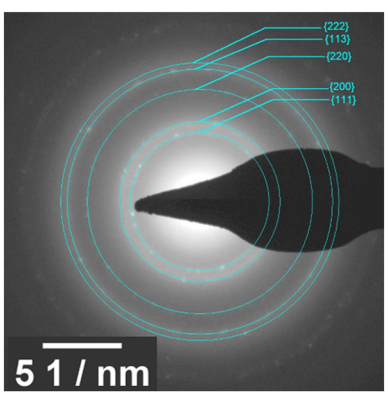

Fig. 2 SAED diffraction pattern of a AuPd nanoparticle supported on activated carbon ROX (AuPd/AC-ROX).

Influence of reaction conditions

In depth exploration into the influence of the reaction conditions, specifically pressure, Na_2CO_3-equivalents, and reaction temperature, was conducted to elucidate their impact on the FDCA yield (Fig. 4). We observed that with AuPd/TiO_2 an increase of the FDCA yield from 60 to 74% occurred while increasing the reaction pressure from 12 to 51 bar. This finding underscores the positive effect of heightened reaction pressure on FDCA production. The molality of oxygen at the reaction temperature of 100 °C is about 0.0008 mol_{O_2} $kg_{H_2O}^{-1}$.[52] The solubility increases almost linearly with escalating reaction pressure, reaching nearly 0.04 mol_{O_2} $kg_{H_2O}^{-1}$ at about 50 bar pressure.[52] The enhanced oxygen solubility is expected to lead to an improved availability of oxygen on the catalyst surface, thereby expediting a fast removal of hydrogen-species from the surface.

Even at a pressure of 12 bar the average HFCA yield and FFCA yield (not shown in graph) were just 2% and 1%, respectively. This indicates that the lower FDCA yield cannot be solely explained by an incomplete conversion of the reaction intermediates. Consequently, the decomposition of HMF is enhanced, which might be attributed to reduced O_2 availability at the active sites, or blockage of active sites by strong adsorption of FDCA and intermediate products.

Table 2 HMF conversions and FDCA yields over AuPd/ZrO_2, AuPd/TiO_2, and AuPd/AC-ROX in batch-mode HMF oxidation (0.1 M HMF, 100 °C, 15 bar air, 2 eq. Na_2CO_3, 5 h, M (metal = Au + Pd) : HMF 1 : 92)

Catalyst	HMF conversion/%	FDCA yield/%
AuPd/ZrO_2	>99	94
AuPd/TiO_2	>99	97
AuPd/AC-ROX	>99	>99

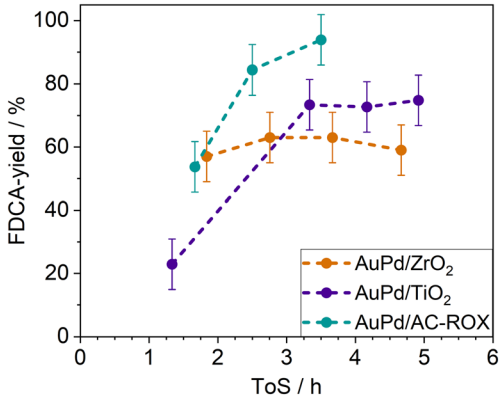

Fig. 3 Support influence on continuous flow HMF oxidation with $AuPd/ZrO_2$ (LHSV: 7.7 min^{-1}), $AuPd/TiO_2$ (LHSV: 5 min^{-1}), AuPd/AC-ROX (LHSV: 1.9 min^{-1}; 0.1 M HMF, 4 eq. Na_2CO_3, 100 °C, 51 ± 3 bar, liquid-flow: 0.1 mL min^{-1}, air-flow: 20 mL min^{-1}).

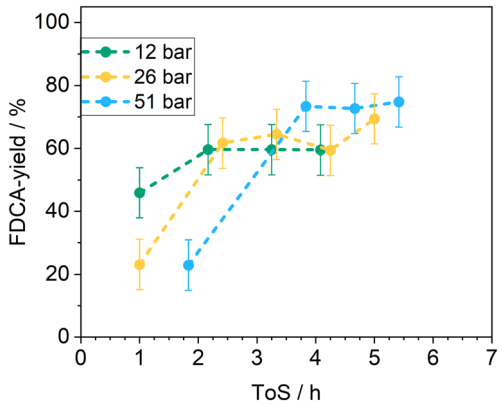

Fig. 4 Pressure influence on the continuous flow HMF oxidation with $AuPd/TiO_2$ (0.1 M HMF, 4 eq. Na_2CO_3, 100 °C, liquid-flow: 0.1 mL min^{-1}, air-flow: 20 mL min^{-1}, LHSV: 5 min^{-1}).

We studied the influence of Na_2CO_3-equivalents added to the reaction solution (Fig. 5). For $AuPd/TiO_2$, we observed a significant increase of the FDCA yield from 39% to 74%, after >4 h ToS, when transitioning from two to four equivalents of Na_2CO_3. A further increase to six equivalents of Na_2CO_3 gave a FDCA yield of 71%. The reason for this effect was attributed to the higher solubility of FDCA when a higher concentration of Na_2CO_3 was dosed. A similar influence was observed when AuPd/AC-ROX served as the catalyst, demonstrating a linear FDCA yield increase up to 100% at about 3.5 h ToS. Afterwards the catalyst showed a linear decrease in FDCA yield until the end of the experiment, suggesting deactivation likely due to FDCA precipitation on active sites at elevated FDCA-concentration.

In the experiment employing six equivalents of Na_2CO_3, no linear decrease of the FDCA yield was noticed, resulting in an impressive average FDCA yield of 97%. Notably, neither HFCA, FFCA, nor humins were detected in the product solution in either case. Hence, the deactivation of the catalyst was attributed solely to the precipitation of FDCA on the catalyst surface, with the oxidation of the intermediates proceeding sufficiently rapidly. These findings suggest that to avoid blocking of active sites and product inhibition by FDCA precipitation, it is recommended to use at least six equivalents of Na_2CO_3 (0.6 M) in the HMF-oxidation. Notably, the Na_2CO_3 concentration required for continuous flow operation is three to six times higher than that needed for the batch process.[21] This divergence may be attributed to the short residence time of reactants and products in the continuous flow reactor, which, unlike in the batch process, leads to product inhibition by active site blocking. The solubility of FDCA strongly depends on the pH of the solution, with alkaline solution resulting in the formation of a Na-carboxylate, which was reported to have a higher solubility compared to the carboxylic acid.[53] Thus, the higher concentration of the sodium base enhances the formation rate of the Na-salt of FDCA, which is important under the short residence time compared to the long contact time in batch, avoiding a strong adsorption of the carboxylic acid on the catalyst surface.[54] This disparity underscores the importance of tailoring the reaction conditions to the specific

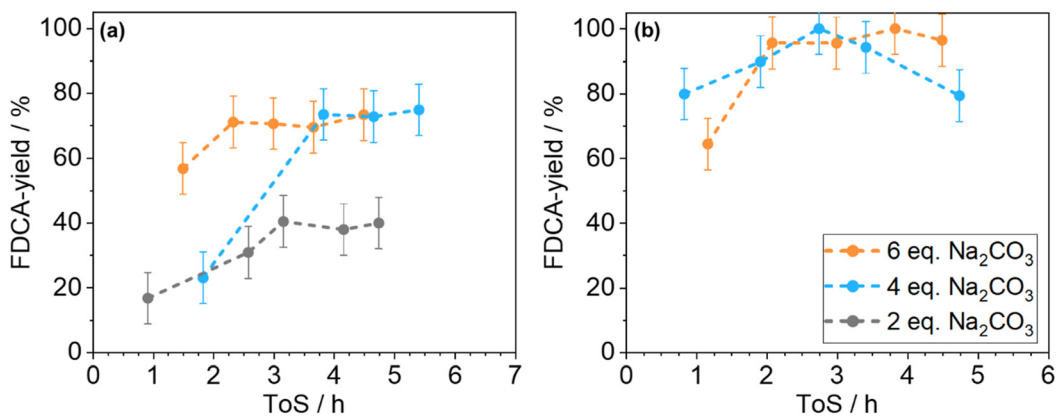

Fig. 5 Influence of quantity of Na_2CO_3-equivalents on the continuous flow oxidation of HMF with (a) $AuPd/TiO_2$ (0.1 M HMF, 100 °C, 51 ± 3 bar, liquid-flow: 0.1 mL min^{-1}, air-flow: 20 mL min^{-1}, LHSV: 5 min^{-1}) and (b) AuPd/AC-ROX (0.1 M HMF, 100 °C, 65 ± 3 bar, liquid-flow: 0.18 mL min^{-1}, air-flow: 20 mL min^{-1}, LHSV: 3.4 min^{-1}).

characteristics of the continuous flow system for optimal catalytic performance.

In the investigation of temperature influence using AuPd/AC-ROX, a higher LHSV was employed, given the proximity of the FDCA yield to 100% in the initial experiments. We observed an augmentation in FDCA yield with increasing reaction temperature, reaching a maximum of 81% at 120 °C (Fig. 6). Subsequently, at an even higher temperature of 135 °C, a slightly lower average FDCA yield of 72% was obtained. However, a linear decrease in FDCA yield was observed after 3.5 h of reaction time (*cf.* Fig. S6†). This decline in FDCA yield might be attributed to the formation of humins resulting from the decomposition of HMF at elevated temperatures, and their deposition on the active sites of the catalyst likely contributed to the steady deactivation of the catalyst. At 80 °C the average FDCA yield was only 29%, underscoring the need for elevated temperatures in this catalytic process.

Interestingly, the combination of 100 °C and the higher LHSV allowed for the monitoring of the yields of reaction intermediates such as HFCA and FFCA. The time-dependent yields of HFCA, FFCA, and FDCA as well as the HMF conversion are shown in Fig. S7 in the ESI.† An average HFCA yield of 20% and a FFCA yield of 12% were obtained at 100 °C. Hence, HFCA emerged as the main intermediate, and the rate-determining step was identified as the oxidation of the alcohol function.[6,19] However, the FFCA yield was not significantly lower, suggesting a comparable rate of FFCA to FDCA oxidation to the oxidation of the alcohol-function in HFCA under our reaction conditions. Continuous flow operation would offer a suitable platform for more detailed kinetic and mechanistic investigations into the oxidation of HMF in future studies.

The achievement of an 81% FDCA yield at 120 °C and a LHSV of 31.4 min^{-1} corresponds to an impressive productivity of 68 mol_{FDCA} mol_{AuPd}^{-1} h^{-1}. These values surpassed those reported in other studies for the continuous flow oxidation of HMF with noble metal-based catalysts (*cf.* Table 3).[47–49] In addition, the productivity exceeded previously published values for optimized batch processes for HMF oxidation, *e.g.* using Au/ZrO_2 with a productivity of 67 mol_{FDCA} mol_{AuPd}^{-1} h^{-1}.[19] Considering that after a reaction in a batch process there is a dead time for draining, cleaning, and reloading the reactor, as well as reactivation of the catalyst, the time-dependent productivity is even higher for a continuous process. Table 3 provides a comparison of productivity values for various continuous and batch processes for HMF oxidation. It is essential to note that the results for the batch process are solely based on the reaction itself and do not include the dead time of the process.

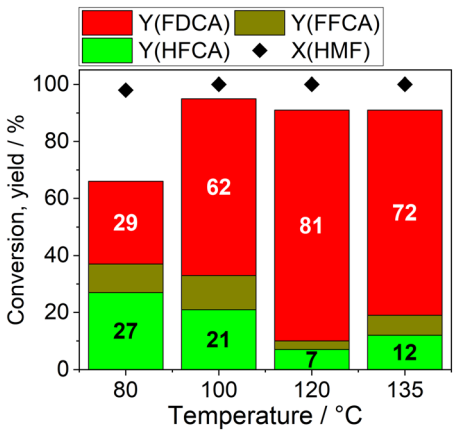

Fig. 6 Temperature influence on the continuous flow oxidation of HMF with AuPd/AC-ROX (0.1 M HMF, 6 eq. Na_2CO_3, 55 ± 5 bar, liquid-flow: 0.22 mL min^{-1}, air-flow: 20 mL min^{-1}, LHSV: 31.4 min^{-1}). The average yields and conversion are shown.

Long-term studies on the catalyst stability

Investigations into catalyst stability were undertaken through a long-term >90 h ToS experiment with AuPd/AC-ROX (0.1 M HMF, 6 eq. Na_2CO_3, 100 °C, 61 ± 5 bar, liquid-flow: 0.22 mL min^{-1}, air-flow: 20 mL min^{-1}, LHSV: 19.6 min^{-1}), to assess the stability of the catalyst under continuous operation over multiple days (Fig. 7). The FDCA yield increased to >90% in the initial reaction hours, but then stabilized at an average of about 75% after the first night (ToS > 16 h). This decrease at the beginning might be caused by the setting of an equilibrium of surface adsorbates on the catalyst in the first hours, leading to the formation of a steady state. In the following days, we recognized a considerable fluctuation in FDCA yields at different measurements over the day. This occurred due to pulsing in the HMF-stream caused by a pump-induced pulsation. Deposition of minor solid residues in the HMF-feed might have caused the pulsing effect of the pump, leading to the observed variations. Hence, the average FDCA yields were determined for each day and the entire 90 h experiment (*cf.* Fig. 7), and the daily average yields are reported in Table S1.† No decline in FDCA yield was observed after 90 h of continuous operation, affirming the high stability of AuPd/AC-ROX in the reaction medium and under the specified conditions. This persistent stability allowed for the continuous production of FDCA in high selectivity. Over the course of the experiment, the average FDCA yield over 90 h ToS was 75% (±12%), which corresponds to a high productivity of 39 mol_{FDCA} mol_{AuPd}^{-1} h^{-1}.

The intermediates HFCA and FFCA were formed with an average yield of 13% and 3%, respectively, over the course of 90 h ToS experiment. The remaining 9% might be attributed to either overoxidation of HMF to CO_2 or degradation of HMF. By adjusting the catalyst mass in the reactor, achieving operation at complete conversion of all intermediate oxidation products is feasible, ensuring a high selectivity to FDCA for at least 90 h without any detectable catalyst deactivation.

To test the stability of the catalyst properties, a spent AuPd/AC-ROX catalyst after oxidation of HMF (0.1 M HMF, 6 eq. Na_2CO_3, 100 °C, 67 ± 5 bar, LHSV: 31.4 min^{-1}, 6 h time on stream) was characterized by XRD (Fig. S8†) and

Table 3 Obtained FDCA yields, productivity, and LHSV values compared with those reported in the literature (M: active noble metal component) for a) continuous processes and b) batch processes

Catalyst	FDCA yield/%	Productivity/mol_{FDCA} mol_M^{-1} h^{-1}	LHSV/min^{-1}	Reference
a) Continuous process				
AuPd/AC-ROX	81	68	31.4	This work
AuPd/TiO_2	74	3.8	5	This work
AuPd/ZrO_2	61	3.1	7.7	This work
Ru/Al_2O_3	63	0.2	1	48
Pt/Al_2O_3	>99	—	4.5	47
Pt/C	99	2.2	—	49
Ru/C[a]	47	1.4	—	55
b) Batch processes				
AuPd/CNT	99	8[b]	—	37
AuPd/ZOC	>99	25[b]	—	56
AuPd/IRA-743	93	0.4[b]	—	57
Au/ZrO_2	89	67[b]	—	19
Au/HY	>99	18[b]	—	23

[a] 6.5 wt% H_2O_2 as an oxidant. [b] Does not include dead time.

adsorption of HMF and FFCA (Table S3†). The AuPd alloy showed a good stability with no indications of phase segregation in XRD. Slight sintering of AuPd was observed, however, the high stability over 90 h ToS indicates that this is not a major cause of deactivation. A high capacity for the adsorption of HMF was retained, indicating a good stability of the activated carbon under reaction conditions. The results are described in detail in the ESI.†

To simulate catalyst deactivation by the formation of humins, another long-term study (0.1 M HMF, 6 eq. Na_2CO_3, 100 °C, 58 ± 4 bar, liquid-flow: 0.22 mL min^{-1}, air-flow: 20 mL min^{-1}, LHSV: 19.6 min^{-1}) was conducted over 50 h ToS. To allow for the formation of humins in the zone prior to the catalyst bed and within the reactor, the flow was intentionally paused after 16 h for about 4 h (Fig. 8). Prior to the deactivation of the catalyst, the FDCA yield was about 87%. After the deactivation of the catalyst by humins, the FDCA yield steadily decreased over the next 35 h, stabilizing at a final yield of about 42%. At the same time, the HFCA yield gradually increased, reaching a final value of 38%. Interestingly, the FFCA yield remained stable over the 35 h period, averaging 12%. Hence, the decline in FDCA yield was attributed to a slower oxidation of the alcohol function of HFCA. The FDCA yield in this scenario was considerably lower compared to the 90 h experiment, underlining how the decomposition of HMF and the formation of humins can result in catalyst deactivation. These observations emphasize the importance of operating continuous flow oxidation of HMF under conditions that favour high selectivity towards the oxidation products while suppressing humin formation,

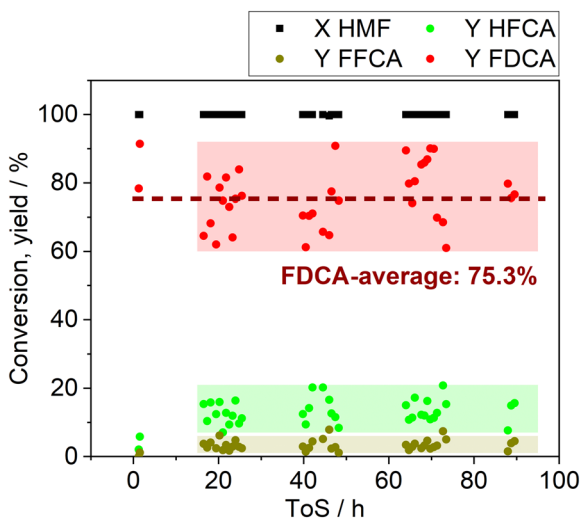

Fig. 7 HMF oxidation with AuPd/AC-ROX (0.1 M HMF, 6 eq. Na_2CO_3, 58 ± 5 bar, liquid-flow: 0.22 mL min^{-1}, air-flow: 20 mL min^{-1}, LHSV: 19.6 min^{-1}). The dashed line represents the average FDCA yield over 90 h ToS. The average FDCA yield for the complete experiment is given in the graph.

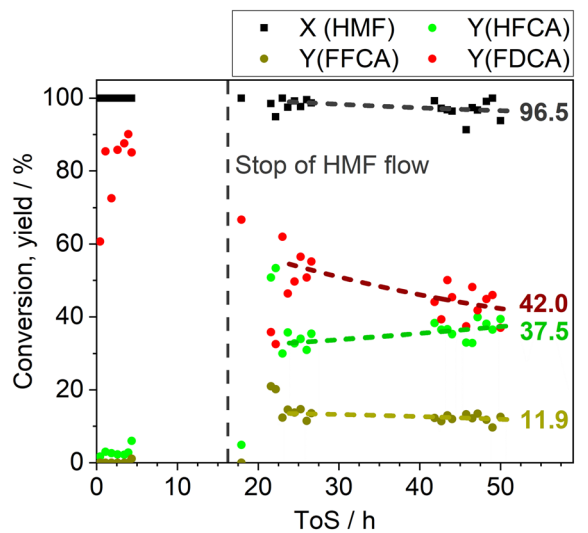

Fig. 8 HMF oxidation with AuPd/AC-ROX (0.1 M HMF, 6 eq. Na_2CO_3, 58 ± 5 bar, liquid-flow: 0.22 mL min^{-1}, air-flow: 20 mL min^{-1}, LHSV: 19.6 min^{-1}). The flow was stopped at the dashed line for about 4 h to induce the formation of humins in the reactor. Dashed lines represent the fitted average conversion and yields.

rather than pursuing the highest possible short-term productivity. Such an approach ensures the long-term stability of the catalyst in the continuous flow process.

Conclusions

The utilization of AuPd-alloys supported on activated carbon exhibited remarkable efficiency in the continuous flow oxidation of HMF, yielding the renewable monomer FDCA. Transitioning to a continuous process offers notable advantages regarding green chemistry, leveraging superior heat and mass transfer, easier scalability, and improved safety through the use of smaller reactor volumes. The achieved productivity, reaching up to 68 mol_{FDCA} mol_{AuPd}^{-1} h^{-1}, surpassed existing benchmarks for continuous flow HMF oxidation by an order of magnitude. Moreover, this productivity level was comparable to optimized batch processes for HMF oxidation. The absence of significant dead time, characteristic of batch processes due to draining and filling of the reactor, positions continuous flow operation at these productivity rates as a promising alternative for HMF oxidation with heterogeneous catalysts.

The AuPd/AC-ROX catalyst demonstrated robust activity and stability over 90 h ToS, establishing AuPd alloys as well-suited catalysts for continuous processes. This investigation addresses a critical gap in current knowledge, shedding light on the durability and robustness of the AuPd-based catalysts under continuous flow conditions, thereby contributing valuable insights to the broader scientific community and advancing the prospects of sustainable monomer synthesis. Future investigations should delve into a comprehensive assessment and optimization of internal and external mass transport limitations for such a continuous process to facilitate up-scaling. In addition, efforts should focus on increasing the maximum concentration of HMF in the feed. The study also revealed steady catalyst deactivation due to the formation of humins in the feed and their adsorption on the catalyst's surface. Hence, meticulous selection of reaction conditions and feed composition is imperative to suppress humin formation. In summary, the continuous flow oxidation of HMF emerges as a promising approach to up-scaling of the oxidation process, offering potential applications in decentralized plants crucial for converting agricultural by-products into important bio-based monomers.

Author contributions

The manuscript was written through contributions of all authors. D. Neukum worked on the conceptualization, investigation, visualization, and writing the original draft. M. E. Ludwig worked on the investigation. A. R. Lakshmi Nilayam helped with investigation. A. Vadarlis helped with build-up of the infrastructure. J.-D. Grunwaldt worked on the project administration, resources, and supervision. E. Saraçi took care of the project administration, resources, visualization, and supervision. All authors contributed to review & editing. All authors have given approval to the publication of the manuscript.

Conflicts of interest

There are no conflicts to declare.

Acknowledgements

The authors would like to thank Veronika Holderied for assistance in HPLC analysis, Armin Lautenbach for ICP-OES analysis, and Shweta Sharma for assistance in conducting STEM. We thank Nikolaos Boukis for provision of a fume hood and help with the construction of the continuous flow setup. STEM imaging was carried out with the support of the Karlsruhe Nano Micro Facility (KNMFi, **https://www.knmf.kit.edu**), a Helmholtz Research Infrastructure at Karlsruhe Institute of Technology (KIT, **https://www.kit.edu**). This work was financially supported by the Federal Ministry of Food and Agriculture (BMEL) through the FNR (Fachagentur Nachwachsende Rohstoffe e. V.) based on a decision taken by the German Bundestag (funding no. 22010718).

References

1 M. Sajid, X. Zhao and D. Liu, *Green Chem.*, 2018, **20**, 5427–5453.
2 R. A. Sheldon, *ACS Sustainable Chem. Eng.*, 2018, **6**, 4464–4480.
3 P. N. R. Vennestrøm, C. M. Osmundsen, C. H. Christensen and E. Taarning, *Angew. Chem., Int. Ed.*, 2011, **50**, 10502–10509.
4 K. Hengst, M. Schubert, W. Kleist and J.-D. Grunwaldt, *Catalytic Hydrogenation for Biomass Valorization*, 2014, pp. 125–150.
5 C. H. Christensen, J. Rass-Hansen, C. C. Marsden, E. Taarning and K. Egeblad, *ChemSusChem*, 2008, **1**, 283–289.
6 O. Casanova, S. Iborra and A. Corma, *ChemSusChem*, 2009, **2**, 1138–1144.
7 E. Taarning, I. S. Nielsen, K. Egeblad, R. Madsen and C. H. Christensen, *ChemSusChem*, 2008, **1**, 75–78.
8 S. Albonetti, T. Pasini, A. Lolli, M. Blosi, M. Piccinini, N. Dimitratos, J. A. Lopez-Sanchez, D. J. Morgan, A. F. Carley, G. J. Hutchings and F. Cavani, *Catal. Today*, 2012, **195**, 120–126.
9 W. Partenheimer and V. V. Grushin, *Adv. Synth. Catal.*, 2001, **343**, 102–111.
10 R.-J. van Putten, J. C. van der Waal, E. de Jong, C. B. Rasrendra, H. J. Heeres and J. G. de Vries, *Chem. Rev.*, 2013, **113**, 1499–1597.
11 A. F. Sousa, C. Vilela, A. C. Fonseca, M. Matos, C. S. R. Freire, G.-J. M. Gruter, J. F. J. Coelho and A. J. D. Silvestre, *Polym. Chem.*, 2015, **6**, 5961–5983.
12 E. de Jong, M. A. Dam, L. Sipos and G. J. M. Gruter, in *Biobased Monomers, Polymers, and Materials*, American Chemical Society, 2012, ch. 1, vol. 1105, pp. 1–13.
13 S. Hameed, L. Lin, A. Wang and W. Luo, *Catalysts*, 2020, **10**, 120.

14 A. Messori, A. Fasolini and R. Mazzoni, *ChemSusChem*, 2022, **15**, e202200228.
15 D. Troiano, V. Orsat and M.-J. Dumont, *ACS Catal.*, 2020, **10**, 9145–9169.
16 D. Astruc, F. Lu and J. R. Aranzaes, *Angew. Chem., Int. Ed.*, 2005, **44**, 7852–7872.
17 D. Zhao, T. Su, Y. Wang, R. S. Varma and C. Len, *Mol. Catal.*, 2020, **495**, 111133.
18 P. Pal and S. Saravanamurugan, *ChemSusChem*, 2019, **12**, 145–163.
19 O. R. Schade, K. F. Kalz, D. Neukum, W. Kleist and J.-D. Grunwaldt, *Green Chem.*, 2018, **20**, 3530–3541.
20 H. Ait Rass, N. Essayem and M. Besson, *Green Chem.*, 2013, **15**, 2240–2251.
21 D. Neukum, L. Baumgarten, D. Wüst, B. B. Sarma, E. Saraçi, A. Kruse and J.-D. Grunwaldt, *ChemSusChem*, 2022, **15**, e202200418.
22 N. K. Gupta, S. Nishimura, A. Takagaki and K. Ebitani, *Green Chem.*, 2011, **13**, 824–827.
23 J. Cai, H. Ma, J. Zhang, Q. Song, Z. Du, Y. Huang and J. Xu, *Chem. – Eur. J.*, 2013, **19**, 14215–14223.
24 X. Han, C. Li, Y. Guo, X. Liu, Y. Zhang and Y. Wang, *Appl. Catal., A*, 2016, **526**, 1–8.
25 S. Siankevich, G. Savoglidis, Z. Fei, G. Laurenczy, D. T. L. Alexander, N. Yan and P. J. Dyson, *J. Catal.*, 2014, **315**, 67–74.
26 A. H. Motagamwala, W. Won, C. Sener, D. M. Alonso, C. T. Maravelias and J. A. Dumesic, *Sci. Adv.*, 2018, **4**, 9722.
27 B. Siyo, M. Schneider, M.-M. Pohl, P. Langer and N. Steinfeldt, *Catal. Lett.*, 2014, **144**, 498–506.
28 Y. Wang, K. Yu, D. Lei, W. Si, Y. Feng, L.-L. Lou and S. Liu, *ACS Sustainable Chem. Eng.*, 2016, **4**, 4752–4761.
29 J. Artz and R. Palkovits, *ChemSusChem*, 2015, **8**, 3832–3838.
30 C. M. Pichler, M. G. Al-Shaal, D. Gu, H. Joshi, W. Ciptonugroho and F. Schüth, *ChemSusChem*, 2018, **11**, 2083–2090.
31 Y. Y. Gorbanev, S. Kegnæs and A. Riisager, *Top. Catal.*, 2011, **54**, 1318.
32 D. Zhao, D. Rodríguez-Padrón, R. Luque and C. Len, *ACS Sustainable Chem. Eng.*, 2020, **8**(23), 8486–8495.
33 O. R. Schade, A. Gaur, A. Zimina, E. Saraçi and J.-D. Grunwaldt, *Catal. Sci. Technol.*, 2020, **10**, 5036–5047.
34 A. Villa, M. Schiavoni, S. Campisi, G. M. Veith and L. Prati, *ChemSusChem*, 2013, **6**, 609–612.
35 O. R. Schade, F. Stein, S. Reichenberger, A. Gaur, E. Saraçi, S. Barcikowski and J.-D. Grunwaldt, *Adv. Synth. Catal.*, 2020, **362**, 5681–5696.
36 G. Uzunidis, O. Schade, D. Schild, J.-D. Grunwaldt and S. Behrens, *ChemNanoMat*, 2021, **7**, 1108–1116.
37 X. Wan, C. Zhou, J. Chen, W. Deng, Q. Zhang, Y. Yang and Y. Wang, *ACS Catal.*, 2014, **4**, 2175–2185.
38 D. Bonincontro, A. Lolli, A. Villa, L. Prati, N. Dimitratos, G. M. Veith, L. E. Chinchilla, G. A. Botton, F. Cavani and S. Albonetti, *Green Chem.*, 2019, **21**, 4090–4099.
39 M. K. Jha, J.-C. Lee, M.-S. Kim, J. Jeong, B.-S. Kim and V. Kumar, *Hydrometallurgy*, 2013, **133**, 23–32.
40 S. E. Davis, B. N. Zope and R. J. Davis, *Green Chem.*, 2012, **14**, 143–147.
41 X. Han, L. Geng, Y. Guo, R. Jia, X. Liu, Y. Zhang and Y. Wang, *Green Chem.*, 2016, **18**, 1597–1604.
42 L. Wan, M. Jiang, D. Cheng, M. Liu and F. Chen, *React. Chem. Eng.*, 2022, **7**, 490–550.
43 C. Wiles and P. Watts, *Eur. J. Org. Chem.*, 2008, **2008**, 1655–1671.
44 D. Dallinger and C. O. Kappe, *Curr. Opin. Green Sustainable Chem.*, 2017, **7**, 6–12.
45 R. Gérardy, D. P. Debecker, J. Estager, P. Luis and J.-C. M. Monbaliu, *Chem. Rev.*, 2020, **120**, 7219–7347.
46 F. Gomollón-Bel, *Chemistry International*, 2019, **41**, 12–17.
47 M. A. Lilga, R. T. Hallen and M. Gray, *Top. Catal.*, 2010, **53**, 1264–1269.
48 A. Danielli da Fonseca Ferreira, M. Dorneles de Mello and M. A. P. da Silva, *Ind. Eng. Chem. Res.*, 2019, **58**, 128–137.
49 F. Liguori, P. Barbaro and N. Calisi, *ChemSusChem*, 2019, **12**, 2558–2563.
50 Z. Gao, R. Xie, G. Fan, L. Yang and F. Li, *ACS Sustainable Chem. Eng.*, 2017, **5**, 5852–5861.
51 D. Neukum, E. Saraci, B. Krause, A. R. L. Nilayam, A. Sinigalia and J.-D. Grunwaldt, *ChemCatChem*, 2024, e202301228.
52 M. Geng and Z. Duan, *Geochim. Cosmochim. Acta*, 2010, **74**, 5631–5640.
53 B. S. Rao, M. J. Hidajat, G.-N. Yun and D. W. Hwang, *Catal. Sci. Technol.*, 2023, **13**, 6921–6936.
54 W. Xie, H. Liu, X. Tang, X. Zeng, Y. Sun, X. Ke, T. Li, H. Fang and L. Lin, *Appl. Catal., A*, 2022, **630**, 118463.
55 D. Zhao, D. Rodriguez-Padron, K. S. Triantafyllidis, Y. Wang, R. Luque and C. Len, *ACS Sustainable Chem. Eng.*, 2020, **8**, 3091–3102.
56 Z. Gui, W. Cao, S. Saravanamurugan, A. Riisager, L. Chen and Z. Qi, *ChemCatChem*, 2016, **8**, 3636–3643.
57 C. A. Antonyraj, N. T. T. Huynh, S.-K. Park, S. Shin, Y. J. Kim, S. Kim, K.-Y. Lee and J. K. Cho, *Appl. Catal., A*, 2017, **547**, 230–236.

